Optics Communications 297 (2013) 176–181

Contents lists available at SciVerse ScienceDirect

Optics Communications

journal homepage: www.elsevier.com/locate/optcom

Comprehensive optical study of the dragonfly *Aeshna cyanea* transparent wing

K.A. Dompreh [a,c,d,*], M.J. Eghan [d], L. Kotsedi [a,c], M. Maaza [a,b,c]

[a] *Nanosciences African Network (NANOAFNET), iThemba LABS-National Research Foundation, 1 Old Faure road, Somerset West 7129, P.O. Box 722, Somerset West, Western Cape Province, South Africa*

[b] *UNESCO-UNISA Africa Chair in Nanosciences/Nanotechnology, College of Graduate Studies, South Africa*

[c] *University of South Africa (UNISA), Muckleneuk ridge, P.O. Box 392, Pretoria- South Africa*

[d] *Department of Physics, University of Cape Coast, Ghana*

ARTICLE INFO

Article history:
Received 23 February 2012
Accepted 14 January 2013
Available online 1 February 2013

Keywords:
Pruinosity
Odonatan
Surface equivalent principle
Relative refractive index
Nystrom Matrix

ABSTRACT

The optical properties of the transparent wings of the Dragonfly *Aeshna cyanea* were studied using a comprehensive set of optical measurements, experimental analysis and theoretical modeling which involves the use of a high level programming language to simulate the optical effects seen. With these, the relative refractive index of the Odonatan wing, the pruinosity associated with the microstructure and the chemical composition of the wings were studied. The Nystrom matrix techniques were applied to solve the surface currents J_Z and H_Z of the scattered fields for different incident angles from grazing and used to explain the pruinosity associated with the wings microstructure. The wing was found to be an Electro-Optic Material (EOM) associated with a number of Nonlinear Optical (NLO) responses having high frequency absorption for extreme UV and also, leaky multi-channeling wave guide.

1. Introduction

The Dragonfly *Aeshna cyanea* (Anisoptera, Aeshnidae) is an insect belonging to the infraorder Anisoptera of the order Odonatan [1]. Scientific interest in the study of its wings stern from the various structural [2] and optical properties [3] associated with it. Typically, the framework of the Odonatan wing consists mainly of a three-dimensional skeletal network, predominantly interconnected by stiff veins and cell membranes. The wing's archaic venation was studied ([5–7]), whiles detailed optical studies have been done on the transparent wing membrane by adopting the Nevot–Croce method [23] where, the index of refraction of the cuticle layer was deduced to be 1.56 ($\pm$0.01)+0.003i ($\pm$0.001i) [8]. The wings mechanical strength [4], and their communication through their structural colors [2] have been investigated. Other properties such as the fascinating aerodynamics of the Odonatan were investigated ([4,9–11]) where, the performance at low Reynolds number was calculated ([12–14]). The micro-sculpture of the Odonatan wing was studied [15]. Furthermore, numerical analyses of the structural functions of insect wings under loading regimes were performed ([16–19]). In this paper, the Nonlinear Optical (NLO) properties of the transparent wing of the dragonfly *Aeshna cyanea* are investigated where: (I) the Surface Equivalent Principle –(SEP)– ([20,21]) is utilized in solving for the surface currents via the Nystrom matrix [22] since the Nevot–Croce method used by Vukusic et al., was based on the fact that scattering of the Odonatan surface is weak. The surface scattering method adopted is used to study the propagation of waves in and on the wing by calculating Electric Field Integral Equation (EFIE) and the Magnetic Field Integral Equation (MFIE) of the surface currents J_z and H_z for different incident angles from grazing for the transverse electric (TE) and magnetic (TM) fields; (II) the pruinosity and the transparency of the wing membrane are analyzed in relation to the microstructure and the surface roughness of the wing surface, and lastly, (III) the relative refractive index of the wing is calculated.

2. Material and methods

Fresh wings of the dragonfly *Aeshna cyanea* (Anisoptera, Aeshnidae) were obtained in the afternoon and observed under different conditions: (a) In a dark room using a Nikon Digital compound microscope having a high pressure mercury lamp with a UV filter (~340 nm) see (Fig. 1a) showing fluorescence; (b) Under bright field, the pruinosity of the Odonatan wing surface was revealed (see Fig. 1(b))with lengths and angle measurements taken, and (III) The wing was then stored in the dark room for 24hrs and viewed revealing the fiber-like veins (Fig. 1c). The wing was carbon coated in an Emitech K950x high vacuum turbo system and examined using a Nova NonaSEM 230 scanning electron microscope (SEM) at different sections of the ventral surface in Fig. 2(a and b).

* Corresponding author at: Department of Physics, University of Cape Coast, Ghana.
E-mail address: dompreh@tlabs.ac.za (K.A. Dompreh).

0030-4018/$ - see front matter © 2013 Elsevier B.V. All rights reserved.
http://dx.doi.org/10.1016/j.optcom.2013.01.012

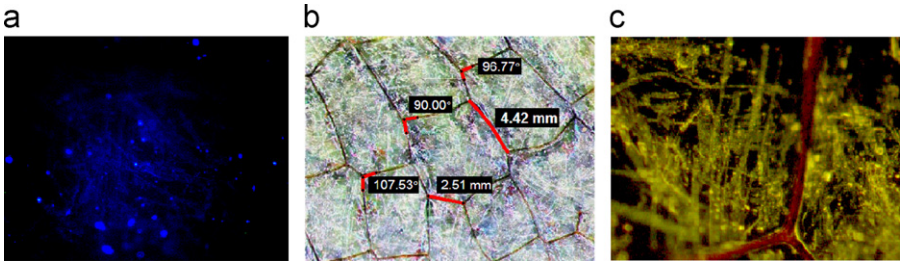

Fig. 1. (a) The fluorescence pattern of the wing. (b) The pruinosity on the wing surface. (c) Fiber-like structures and vein-frame running crosswise in the wing membranes (× 20).

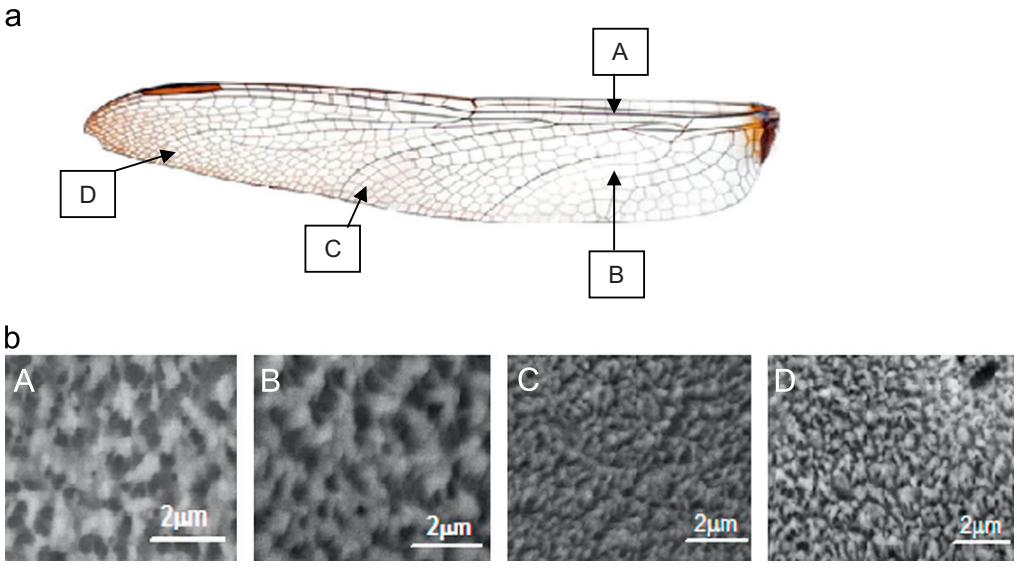

Fig. 2. (a) The ventral view of the wing showing sections (A–D) of the cells which were examined under the SEM. (b) SEM images of the ventral surface of region A on the left to D on the right.

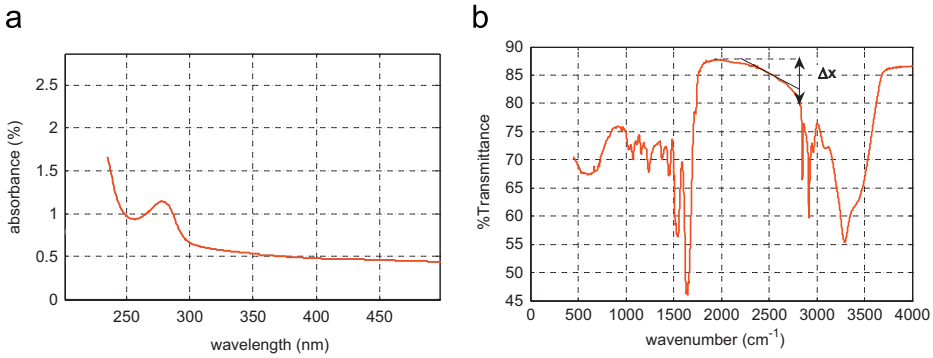

Fig. 3. (a) The nonlinear optical response of the UV–vis-NIR absorption spectral of the wing with absorption at 277 nm indicting C=O with pi-bonds. (b) The FT-IR of the wings having peaks at specific wavenumber.

In addition to the SEM, other spectroscopic measurements were carried out. These includes: (I) the UV–vis–NIR spectroscopy set to a baseline of air [24]; and (II) The Perkin Elmer Fourier Transform Infrared (FT-IR) spectroscopy with the background set to air [25].

3. Results

3.1. UV–vis–NIR

The optical response of the wing was performed by determining the percentage absorption in the UV–vis–NIR wavelength (see Fig. 3a). There was a sharp increase in absorption at 277 nm with an absorption edge at 300 nm indicating a possible C=O chromophores electrons having pi-bonds conjugation. Using a third degree polynomial fit of the transmission (%) data to a wavelength dependant thickness of the wing and calculating the characteristics roots of the polynomial gives the relative refractive index (n_r) of the material as $1.6986 \pm 0.7061i$ (0.33).

3.2. FTIR

The wing is mostly made of chitin where the stretching and bending of bonds was identified using the Fourier Transform Infrared (FTIR) spectrometer. There are peaks which are C–H stretches of CH_3 (2849 cm^{-1}) and CH_2 (2917 cm^{-1}) groups. At 3300 cm^{-1}, the

spectrum showed peaks of independent vibrations of symmetric N–H bonds with different reduced mass due to O–H stretching which is part of either a simple Amine (R_2NH) or an Amide (RCONHR). In the region of 1641 cm^{-1} is the strongest peak belonging to C=O group beyond it is the single bond region referred to as the fingerprint region. The O–H bond stretching which is associated with reduce mass is between 3000 and 4000 cm^{-1}. The indicated slope is linked to the transparency of the material as:

$$\text{Transparent} = \lim_{\Delta x \to 0} |\textit{slope} \text{ of bandwidth}|$$

3.3. Surface roughness analysis

The 3D model of the SEM images A and B in Fig. 3 are presented in Fig. 4 (a,b) with x, y, z (intensity) axes expressed in pixels. This was achieved by interpolating grid points unto the SEM images and viewed at an elevation and azimuthal angle. The two surface plots showed irregular jagged peaks with different spatial orientations which are mostly excess wax on the surface of the wing. Surface roughness modeling was done using the Matlab image processing toolbox [18].

3.4. Surface equivalent principle (SEP)

Assuming a homogenous medium of air surface, characterized by ε_1, μ_1 having the fields E_1,H_1 whiles the wing medium is characterized by ε_2,$\mu_2$and having fields E_2,H_2. The surface currents for both medium are defined as:

$$J_1 = \hat{n} \times H_1, \; K_1 = E_1 \times \hat{n} \tag{1a}$$

$$J_2 = (-\hat{n}) \times H_2, K_2 = E_2 \times (-\hat{n}) \tag{1b}$$

The Helmholtz equation for the electric field is:

$$(\nabla^2 + k^2)E = 0 \tag{2}$$

with $k^2 = \mu\varepsilon\omega^2$. The Electric field can be expressed in terms of the incident and scattered fields as:

$$E = E^{inc} + E^{sc} \tag{3}$$

using the surface equivalent principle [19], the scattered fields can be expressed in term of the surface currents J_z and Henkel function ($H_0^{(1)}$) by utilizing the far field Green function expansion where the point of observation far exceed the source point $|x| >> |x'|$as:

$$E_z^{sc}(\rho,\varphi) = ik_1\eta_1 \frac{e^{i(k_1\rho+\pi/4)}}{2\sqrt{2\pi k_1\rho}} \int_C J_z(x',y') \frac{i}{4} H_0^{(1)}(k_1 r) ds'$$

$$-\frac{\partial}{\partial x}\int_C \sin(\theta') K_t(x',y') \frac{e^{i(k_1\rho+\pi/4)}}{2\sqrt{2\pi k_1\rho}} e^{ik_1(\cos(\varphi)x' + \sin(\varphi)y')} ds'$$

$$+\frac{\partial}{\partial y}\int_C \cos(\theta') K_t(x',y') \frac{e^{i(k_1\rho+\pi/4)}}{2\sqrt{2\pi k_1\rho}} e^{-ik_1(\cos(\varphi)x' + \sin(\varphi)y')} ds' \tag{4}$$

Using the Nystrom matrix, the TE fields for $J_z$can be determined as well as that for $K_z$when Eq. (4) is expressed for TM fields. For completeness, considering $\rho \to \infty$, all terms of order greater than $1/\sqrt{\rho}$ are dropped leaving the φ-dependent factor

$$E_z^{sc}(\rho,\varphi) = \frac{e^{i(k_1\rho+\pi/4)}}{2\sqrt{2\pi k_1\rho}} \left\{ ik_1\eta_1 \int_C J_z(x',y') e^{-ik_1(\cos(\varphi)x' + \sin(\varphi)y')} ds' \right.$$

$$\left. + ik_1 \int_C [\cos(\theta')\sin(\varphi) - \sin(\theta')\cos(\varphi)] K_t(x',y') e^{-ik_1(\cos(\varphi)x' + \sin(\varphi)y')} ds' \right\} \tag{5}$$

Defining the parameters P and Q as:

$$P_i \equiv C_i S_i K_1 \eta_1 e^{i\frac{3\pi}{4}} e^{-iK_1(\cos(\varphi)x_i^1 + \sin(\varphi)y_i^1)}$$

$$Q_i \equiv C_i S_i K_1 \left[\cos\left(\theta_i^1\right)\sin(\varphi) - \sin\left(\theta_i^1\right)\cos(\varphi) e^{i\frac{3\pi}{4}} - e^{-iK_1(\cos(\varphi)x_i^1 + \sin(\varphi)y_i^1)} \right]$$

The scattered field can simply written as:

$$E_z^s(\rho,\varphi) = \frac{e^{ik_1\rho}}{2\sqrt{2\pi k_1\rho}} (P_i J_i + Q_i K_i) = g(\rho) f(\varphi) \tag{6}$$

with i being the Einstein summation

$$g(\rho) = \frac{\exp(iK_1\rho)}{2\sqrt{2\pi K_1\rho}}, f(\varphi) = (P_i J_i + Q_i K_i) \tag{7}$$

The $f(\varphi)$ contains all the angular information whiles $g(\rho)$adjust the phase and normalization of the wave at an arbitrary distance ρ. From Eq. (7), the scattering of light by the wing is modeled by using the surface roughness and waviness values to simulate the wings surface and its relation with the scattered light. Numerical values used in the simulation include the thickness of the scatterer 2.5λ and length$=112\lambda$, the roughness and waviness stated in Table 1. With these the TE and the TM for the plane waves at various angles are presented in Figs. 5 and 6 respectively.

4. Discussion

Optical images of the Wing surfaces are presented in Fig. 1(a–c), and their optical responses indicated under different conditions. The observed trapping of light in the Odonatan wing showed certain characteristics of confinements on the nano level indicating that the pruinosity of the wing is an evanescence of the trap light on a rough surface. Figs. 2 and 3(a–d) shows the SEM

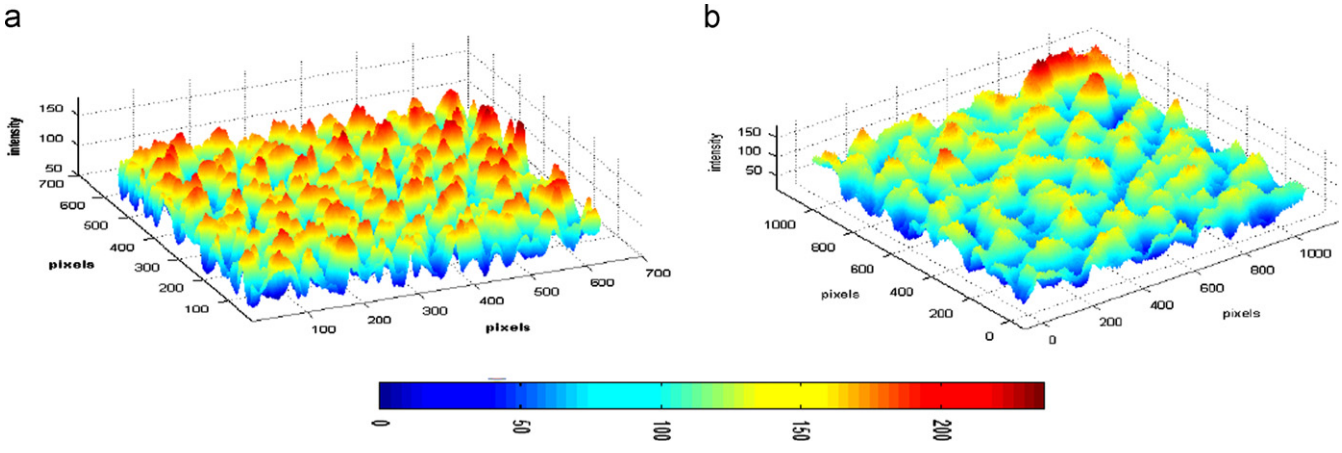

Fig. 4. (a) 3D model of SEM image A. (b) 3D model of SEM image B.

Table 1
The surface roughness R_{aR}, the RMS R_{qR},the skewness (R_{skR}) and Kurtosis (R_{kuR}), waviness—(the average R_{aW}, the RMS R_{qW}, the skewness R_{skW} and R_{kuW}) parameters.

Image	R_{aR}	Surface roughness parameters					R_{skW}	R_{kuW}
		R_{qR}	R_{skR}	R_{kuR}	R_{aW}	R_{qW}		
A	25.10274	31.03239	1.286662	3.079446	96.44383	97.7683	1.033146	1.081768
B	19.83076	24.72870	1.011331	3.146809	91.39780	93.77188	1.066027	1.171204

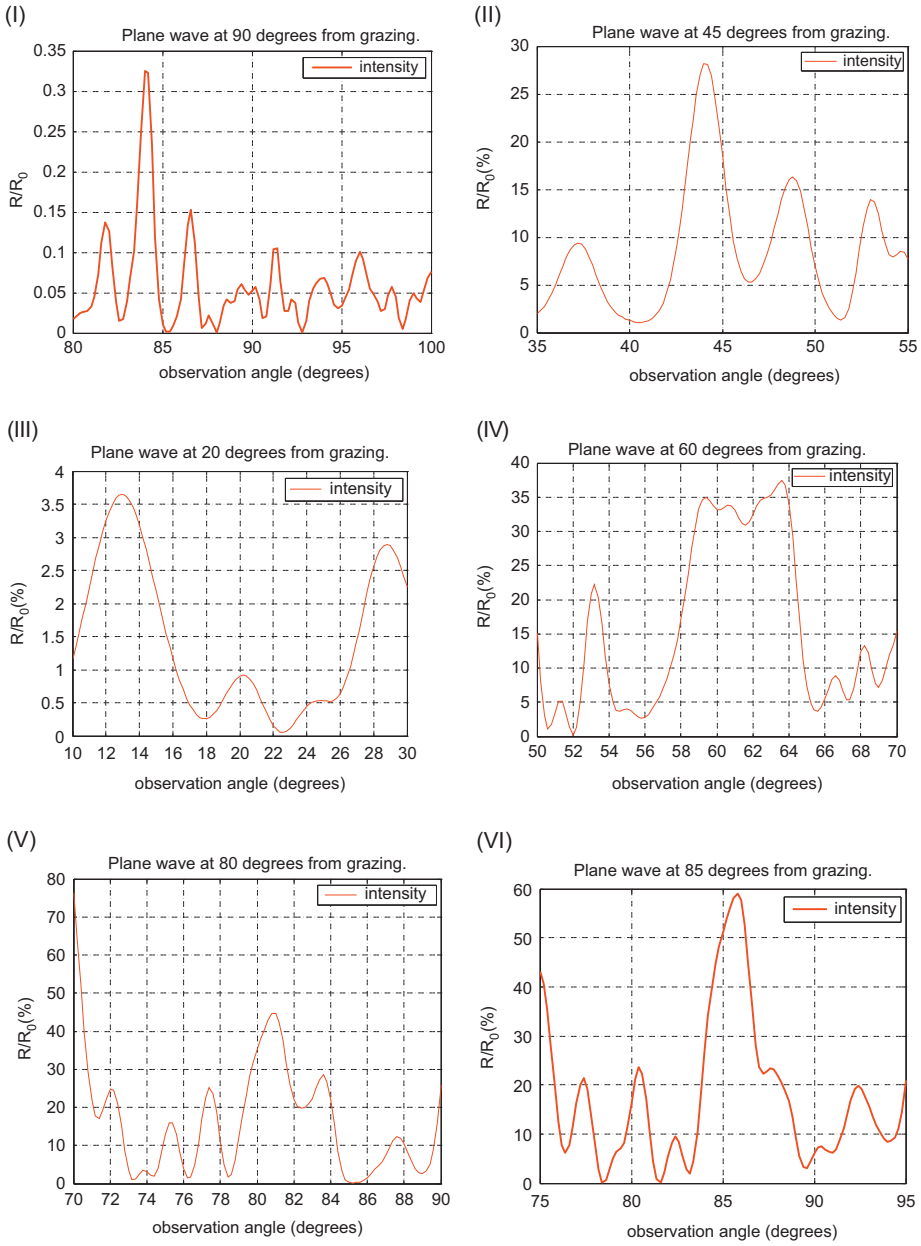

Fig. 5. The measured reflectance plots at various angles of incidence shown in (I)–(VII).

images of the portions of the wing indicating the texture of their surfaces. The roughness of the surfaces of the SEM images varies from point to point. A better comparison of their roughness is seen by modeling the images A and B into 3D form as in Fig. 4(a,b) with their respective roughness and waviness presented in Table 1. The peak regions marked in red indicates excess wax on the surface of the wing. Image A has a high RMS roughness value compared to image B but both have a roughness kurtosis approximately 3 indicating a Gaussian surface. Material characterization from the UV–vis–NIR and the FT-IR are duly presented. The wing absorbs in the UV region at 277 nm with a possible chemical formula of RCONHR having relative refractive index of $1.6986 \pm 0.7061i$ (0.33) where, the complex part indicate the optical absorption of the material. The numerical values (see (Table 1)) are used to model the scattering of electromagnetic waves by the surface of the Odonatan wing. With RMS 0.75 nm

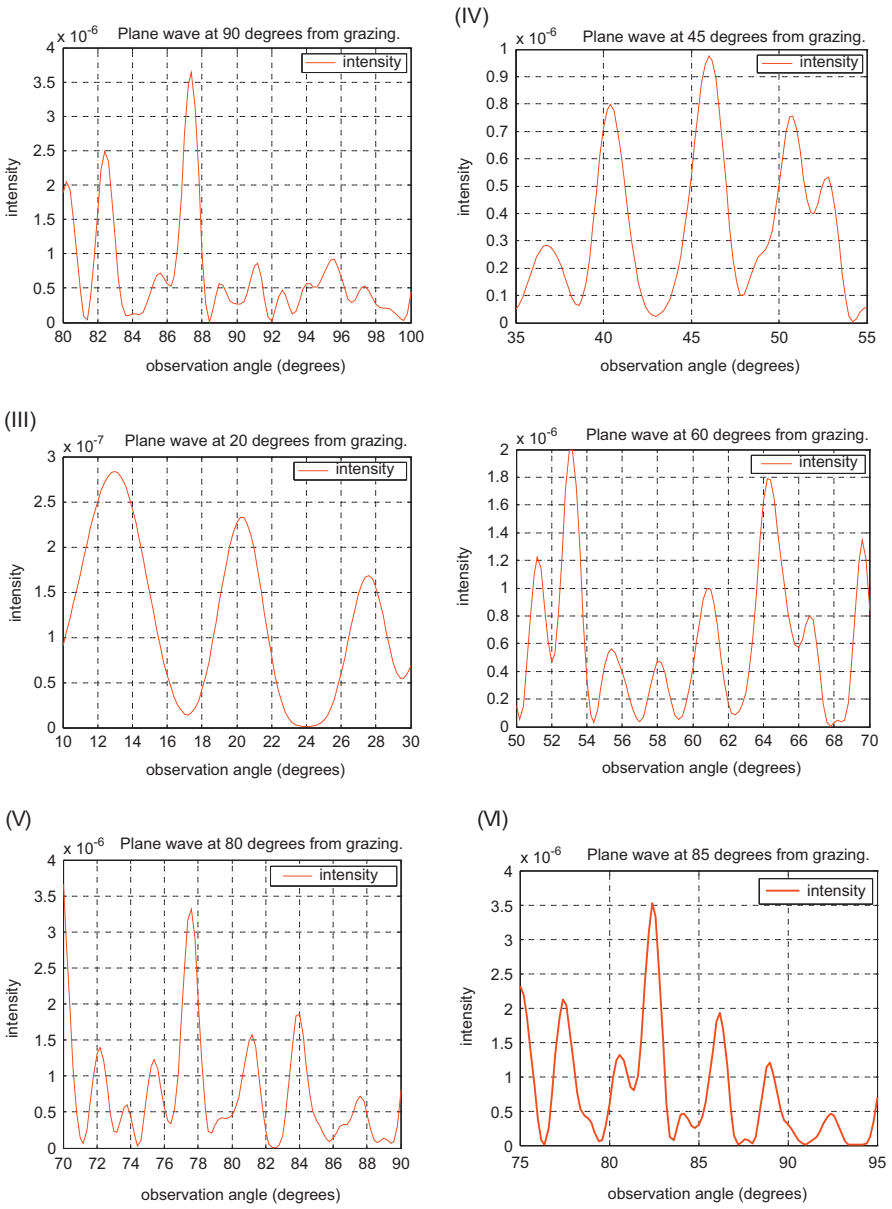

Fig. 6. The measured intensity plot at various angles of incidence shown in (I)–(VII).

Table 2
Numerical values of the TE scattered fields for the Nystrom matrix, matrix inversion and far field intensity.

Degrees from gazing	90°	45°	20°	60°	80°	85°
Nystrom matrix fill	3318.25	1225.03	5646.09	1217.05	1177.5	1325.78
Matrix inversion:	109.016	28.0625	228.578	25.9688	26.1563	25.5
Far field intensit	5.40625	2.79688	7.84375	2.5625	2.45313	2.70313

Table 3
Numerical values of the TM scattered fields for the Nystrom matrix, matrix inversion and far field intensity.

Degrees from gazing	90°	45°	20°	60°	80°	85°
Nystrom matrix fill	1138.11	1148.2	1148.39	1164.2	1175.44	1220.63
Matrix inversion	26.375	26.0156	25.9219	28.625	26.0156	24.75
Far field intensity	2.64063	2.65625	2.70313	2.5625	2.3125	2.70313

(ventral surface) and 0.5 nm (dorsal surface) of image A, the thickness of the scatterer 2.5λ and length 112λ, the measured and calculated reflectance of specified angles are presented in Figs. 5(I–VI) and 6(I–VI) with their corresponding numerical values stated in Tables 2 and 3. These measurements were specifically taken at incident angles from grazing to correspond with the ASTM angles of 20°, 60° and 85° with an additional 45° and 90° measurements. Figs. 5 and 6 are the angle dependant TE and TM scattered waves and from the Nystrom matrix the surface currents can be deduced.

5. Conclusion

The Dragonfly wing is an Electro-Optic Material (EOM) with conjugated molecules possessing UV absorbing chromophores with nonlinear optical properties. The pruinosity associated with the wing surface is due to an evanescence of trapped light traveling along the fiber-like structures and scattered by a rough Gaussian surface with material relative refractive index deduced as 1.6986 ± 0.7061i. The electric fields and magnetic fields in the wing are due to light which causes variation in refractive index variation. This is responsible for the nonlinear optical effect as trapping of light, and the pruinosity of the wing. The pruinosity is a restriction to the transparent constituent materials which ensures that absorption losses are negligible thus the macroscopic linear and nonlinear optical properties of the Odonatan materials in terms of their mesoscopic optical properties depend on the topology of the composite material. The pruinosity of the Odonatan wing surface is associated with the propagation of light in the membrane where the inclusion of light in the host forms a composite with an effective dielectric constant (ε_{eff}). The transparent wings membranes are made of micro-lenses that focus light unto the micro fiber-like structures. Such micro-lenses focuses light unto the fiber –like veins. With these, the wing should exhibit effect such as self-focusing, self-phase modulation and modulation instabilities making it a good source of an optical switch for 3D photonic applications.

Acknowledgments

The work was financially supported by the following organizations: Nanoscience African Network (NANOAFNET), National Research Foundation (NRF), and iThemba LABS of South Africa.

References

[1] P.S. Corbet, Dragonflies: Behavior and Ecology of Odonatan, Cornell University Press, Ithaca, NY, ISBN 0801425921, 1999.
[2] P. Vukusic, J.R. Sambles, Nature 424 (2003) 852.
[3] S.N. Gorb, Journal of Insect Behavior 11 (1998) 73.
[4] R.J. Wootton, Advances in Odonatology 5 (1991) 153.
[5] A.V. Martynov, Russian Entomological Review 18 (1924) 145.
[6] D.J.S. Newman, The Functional Wing Morphology of Some Odonata, Dissertation, University of Exeter, Exeter, 1982.
[7] H.K. Pfau, Tijdtschrift voor Entomologie 129 (1986) 35.
[8] I.R. Hooper, P. Vukusic, R.J. Wootton, Optics Express 4891 (2006) 2006.
[9] G. Rüppell, Journal of Experimental Biology 144 (1989) 13.
[10] J.M. Wakeling, C.P. Ellington, Journal of Experimental Biology 200 (1997) 543.
[11] S.P. Sane, Journal of Experimental Biology 2006 (2003) 4191.
[12] C.J.C. Rees, Nature 256 (1975) 200.
[13] M Okamoto, K Yasuda, A. Azuma, Journal of Experimental Biology 199 (1996) 281.
[14] M. Tamai, Z. Wang, G. Rajagopalan, H. Hu, G. He, Aerodynamic performance of a corrugated dragonfly airfoil compared with smooth airfoils at low Reynolds numbers, in: Proceedings of the 45th AIAA Aerospace Sciences Meeting and Exhibit, Reno, Nevada, 2007, pp. 1–12.
[15] A.B. Kesel, Journal of Experimental Biology 203 (2000) 3125.
[16] M.J.C. Smith, AIAA Journal 34 (1996) 1348.
[17] R.C. Herbert, P.G. Young, C.W. Smith, R.J. Wootton, K.E. Evans, Journal of Experimental Biology 203 (2000) 2945.
[18] S.A. Combes, T.L. Daniel, Journal of Experimental Biology 206 (2003) 2979.
[19] A.B. Kesel, U. Philippi, W. Nachtigall, Computers and Biomedical Research 28 (1998) 423.
[20] A.F Peterson, et al., Computational Methods for Electromagnetics, IEEE Press, New York, 1998.
[21] J. Jensen, Computationally Modeling the Effect of Surface Roughness on Soft X-ray Multilayer Reflectors. Honors Thesis Brigham Young University, Provo, UT, 2006.
[22] R.S. Turley, Using the Nystrom Method to Solve the Scalar Electric Field Integral Equation Brigham Young University Internal Report, 2005.
[23] L. Nevot, P. Croce, Revue de Physique Appliquee 15 (1980) 761.
[24] Skoop, et al., Principles of Instrumental Analysis, 6th ed., Thomson Brooks/Cole, 2007 169 –173.
[25] P. Griffiths, J.A. de Hasseth, Fourier Transform Infrared Spectrometer, 2nd ed., Wiley Blackwell, 2007. ISBN-0471194042.